2007

Reactive Oxygen Emission From Microwave Discharge Plasmas

S. Popovic
Old Dominion University, spopovic@odu.edu

M. Rašković

S. P. Kuo

L. Vuskovic
Old Dominion University, lvuskovi@odu.edu

Original Publication Citation

Popović, S., Rašković, M., Kuo, S. P., & Vušković, L. (2007). Reactive oxygen emission from microwave discharge plasmas. *Journal of Physics: Conference Series, 86*(1),012013 . doi:10.1088/1742-6596/86/1/012013

Journal of Physics: Conference Series **86** (2007) 012013 doi:10.1088/1742-6596/86/1/012013

Reactive Oxygen Emission from Microwave Discharge Plasmas

S Popović,[1] M Rašković,[1] S P Kuo[2] and L Vušković[1]

[1]Department of Physics, Old Dominion University, Norfolk, Virginia 23529, USA

[2]Department of Electrical and Computational Engineering, Polytechnic University, Brooklyn, New York 11201, USA

E-mail: popovic@physics.odu.edu

Abstract. Metastable oxygen atoms and molecules have received increased interest because of their function in surface modification, bio-decontamination and many other industrial applications, in addition to the role in the upper atmospheric layer chemistry. We review work on production and detection of metastable oxygen and we describe our experiments, including the development of techniques for measurement of metastable molecular oxygen. We show that either metastable oxygen molecules or metastable oxygen atoms can be produced in large quantities in electrical discharges, carefully tailored to promote the required kinetics. Although the two species may coexist, colder discharge regimes favor production of molecules, while at higher temperature conditions atomic oxygen prevails. We found that microwave cavity discharges in He/O_2 mixtures favor molecular production, but that an arc-seeded microwave torch in air shows preference of atomic production. Result on the specific yield of molecular oxygen in the microwave cavity discharge shows qualitative agreement with the models.

1. Introduction

We present our results on production and detection of metastable atomic and molecular oxygen species. These oxygen states have long enough lifetimes to be able to produce observable biochemical effects on the atmosphere, solid or liquid surfaces. In this paper we give an overview of the techniques used for detection of singlet oxygen. In addition, we describe the chosen detection technique – the off-axis integrated cavity-output spectroscopy (ICOS) based on laser absorption spectroscopy. ICOS is supported by the in-situ emission spectroscopy for the purpose of characterizing the source of molecular singlet oxygen and of simultaneously correlating oxygen singlet yield with the concentrations of other reactive species in the discharges, such as charged particles and atomic oxygen.

Several types of discharges are discussed with respect to the production and sustaining of the metastable oxygen population. Special emphasis is given to cavity microwave discharges in

helium/oxygen mixtures, where metastable molecular oxygen can be produced efficiently in proportionally large quantities (order of 20% of total oxygen number density) and to the arc-seeded microwave plasma torch, with efficient production of atomic metastable oxygen.

Oxygen molecule has at least four long-living metastable states. Most interesting are the three singlet states, $a^1\Delta_g$ (Oxygen Singlet Delta – OSD), $b^1\Sigma_g^+$ and $c^1\Sigma_u^-$ (Oxygen Singlet Sigma – OSS). Transition from the singlet states to the oxygen ground state, $^3\Sigma_g^-$, represents a magnetic dipole transition (singlet-triplet intercombination). Rather difficult to observe by conventional spectroscopy techniques, these states, especially OSD, have became of increased interest due to their reactivity and important role in a variety of environments, experiments and applications. Here are some of the currently active research topics involving OSD and OSS.

a) Electronic systems involving OSD and OSS as the upper levels are contributing strongly to the radiation transfer in the terrestrial atmosphere. At an altitude of about 70 km up to one sixth of gas heating results from the absorption of solar radiation by molecular oxygen in the red (from ground state to OSS) and near-infrared (to OSD) and subsequent exothermic chemical reactions [1].
b) Oxygen plasmas are involved in a variety of surface reactions of importance for semiconductor industry [2]. For instance, ashing of phototresist films on semiconductor wafers involve OSD and OSS together with the atomic oxygen.
c) Atmospheric pressure plasmas produce large quantities of OSD and OSS with demonstrated decontamination capability of chemical and biological warfare (CBW) agents from relatively large surfaces [3].

In most applications it is of crucial importance to detect, quantify and control the population of OSD. In addition, it is important to correlate the OSD density with populations of other agents present in the environment, such as charged particles and the atomic oxygen. The aim of this work is to contribute to the development of sensitive spectroscopic techniques suitable for quantitative detection of OSD and for correlation with the dynamics of the medium and other reactive agents.

2. Production of OSD in Electrical Discharges

Metastable OSD is produced by (a) chlorinating reaction of the alkaline solution in hydrogen peroxide, (b) photo-dissociation of ozone in Hartley (200-320 nm) and Huggins (300-360 nm) bands and (c) electric discharges via several mechanisms. In the order of energy efficiency, these mechanisms include direct electron impact excitation from ground state, excitation to OSS with subsequent collisional de-excitation, vibrational excitation of ground state and subsequent electron impact excitation, and electron-impact dissociation and associative de-excitation of atomic metastable oxygen. Some of the listed processes continue to produce OSD in the afterglow so that the OSD yield is subsequently higher in the stabilized flow ~100 ms after passing through the discharge.

First observation of OSD produced by an electrical discharge was made by Foner and Hudson [4] in a very long, typically 1 m, U-shaped discharge tube with hollow electrodes, operating at a pressure of several kPa in an a.c. glow regime. In the middle of the discharge tube a capillary with a pinhole were attached, so that the gas was able to flow to mass spectrometer. This discharge was called Wood's discharge [5] and was quite popular half a century ago since in the molecular hydrogen flow it was able to produce atomic hydrogen in quantities (typically order of 0.1%) suitable for atomic hydrogen spectroscopy. Thus, almost all hyperfine structure effects were discovered using this type of discharge. In the OSD production arrangement the Wood's discharge operated in pure oxygen flow at pressure of about 5 kPa. The length of the capillary was about 30 cm, so that the gas was allowed to a transit time of about 50 ms before reaching the pinhole. Mass spectrometer was carefully designed to avoid destruction of oxygen species by collision. In the presence of discharge the appearance potential curves were different than those of "normal oxygen" observed when discharge was off. The threshold was shifted to lower energies by about 0.93 eV and overall curve looked as it was combined of a "normal" O_2 ionization curve and another curve, starting at lower energy (see Fig. 1). Since the

molecular orbital theory predicts an excited state (OSD) with energy 0.98 eV above the ground state, Foner and Hudson concluded that the enhancement of ion current was due to large quantities of OSD produced in a Wood's discharge.

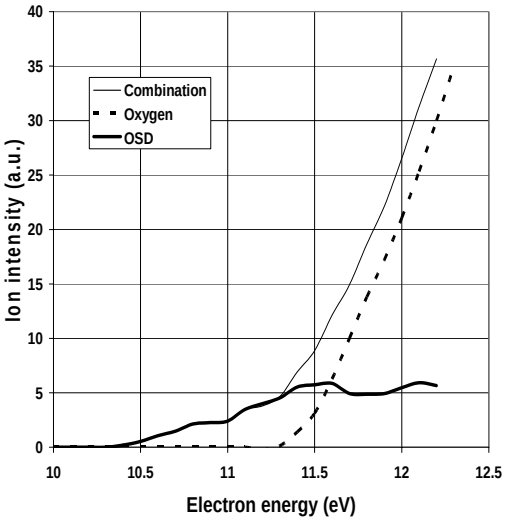

Figure 1. Threshold ionization curves from a Wood's discharge: discharge off, thin solid line; discharge on, dashed line; OSD, thick solid line.

Foner and Hudson have also mentioned without further details that OSD was observed in a radio-frequency discharge at 5 MHz and in a microwave discharge at 2.45 GHz. Wood's discharge has been abandoned since the early studies mostly due to poor efficiency and limited scalability. Modern research employs either electron-beam non-self-sustained discharges or a variety of radio-frequency and microwave self-sustaining discharges. The work is compiled in Table 1, without details on production yields and energy efficiency.

OSD ($a^1\Delta_g$) is the lowest electronically excited state of molecular oxygen with 0.977 eV above the ground state $X^3\Sigma_g^-$ and its most efficient production would occur in discharges where the average electron energy is about 1 eV. It turns out that average electron energy of 1 eV usually occurs at the reduced field values of about 10 Td. Unfortunately, most self-sustained and the e-beam sustained discharges operate at substantially higher reduced electric fields and/or average electron energies. In most cases, the electrons are able to excite higher energy levels of the molecular oxygen, such as $B^3\Sigma_u^-$ or $A^3\Sigma_u^+$ which will then collisionally decay into another metastable state, $c^1\Sigma_u^-$ or to the long-lived $A'^3\Delta_u$ state. All these states have dissociation energy less than 1 eV and could undergo thermal dissociation to form the ground state, $O(^3P)$, or the metastable state, $O(^1D)$. OSD is not present at kinetic temperatures above 2000 K where most of the oxygen is dissociated or reacted, as shown later.

One has to combine oxygen with other gases and apply additional cooling schemes in order to keep low gas-kinetic temperature, scavenge the produced atomic oxygen, and to reduce the ionization threshold. Addition of helium increases the overall degree of ionization, reduces substantially the gas kinetic temperature and increases the residence time in the discharge, which leads to the enhanced presence of molecular oxygen. Indeed, early spectroscopic tables had a separate category of "helium enhanced" molecular bands [6]. Similar effect, but with less intensity, is obtained using argon as the diluent gas. Small amounts of N_2 or NO_2 prevent excessive accumulation of atomic oxygen, and CO or NO were used to enhance ionization in the discharge.

E-beam sustained discharges do not show the efficiency as exceptional as expected in producing OSD, partly due to difficulties in achieving the optimum electron energy at elevated

pressures. Radio-frequency discharges with long afterglows are most often used in the experiments, in spite of relatively large E/N, high average electron temperature and excessive concentration of high energy electrons around the sheaths. Better efficiency has been reported at higher frequencies. Microwave discharges tend to be more efficient producer of OSD, especially at low power density, where gas-kinetic temperature does not exceed 500 K. Combinations of pulsed discharges with small duty cycles and high peak power, like, for example, the "spiker-sustainer" schemes, seem to be even more promising.

At the opposite end are the discharges involving high power density that develop gas-kinetic temperature so high that most Oxygen metastables and the intermediary state become vibrationally excited and easily dissociated. These include sparks, "needles', and torches. Oxygen species in these discharges is predominantly in the atomic state. Therefore, they can be used for efficient production of metastable atomic Oxygen, as discussed later in the paper.

Table 1. Work on OSD production in electrical discharges

First author, year	Discharge	Composition	Technique	Reference
Foner, 1956	a.c. glow (Wood)	pure O_2	experiment	[4]
Benard, 1978	microwave	pure O_2	experiment	[7]
Napartovich, 2001	e-beam non-self-sustaining		concept/model	[8]
Schmiedberger, 2001	low-pressure hollow-cathode radio-frequency jet	$O_2/N_2/NO$ + cold Ar/NO_2 stream	experiment	[9]
Carroll, 2002	pulsed discharge/radio-frequency discharge	O_2 O_2/He	experiment	[10]
Rakhimova, 2003	capacitive radio-frequency	pure O_2, O_2/He or Ar	experiment, model	[11]
Savin, 2003	traveling microwave	pure O_2	experiment, model	[12]
Ionin, 2004	e-beam non-self-sustaining	O_2/Ar with CO, H_2, or D_2	concept/model	[13]
Stafford, 2004	flowing radio-frequency discharges	O_2/He	global kinetic model	[14]
Carroll, 2004, 2005	flowing radio-frequency discharge	O_2/He	experiment	[15,16]
Stafford, 2005	flowing radio-frequency discharges	O_2/He	1D hydrodynamic model	[17]
Arakoni, 2005	flowing radio-frequency discharges	O_2/He	multifluid, 2D hydrodynamic model	[18]
Rawlins, 2005	Evenson cavity microwave	O_2/ He	Experiment	[19]
Pulpytel, 2005	RF-discharge for plasma-assisted CVD	$O_2/Ar/Sn(CH_3)_4$	Experiment	[20]
Carroll, 2005	flowing radio-frequency discharge	$O_2/NO_2/NO$	Experiment	[21]
Babaeva, 2006	High power pulsed/low- power sustaining discharge	O_2 O_2/He	Model	[22]
Verdeyen, 2006	flowing radio-frequency discharge	O_2/He/NO	Experiment	[23]
Ionin, 2006	e-beam non-self-sustaining	O_2/Ar/CO	Experiment/model	[24]
Proshina, 2006	radio-frequency discharge	O_2/HgO coating on tube walls	experiment/model	[25]

A comprehensive review of OSD production research in gaseous and plasma environments has been recently published [26]. Pulpytel *et al.* [20] reported that the maximum density of OSD (10-15%) has been observed at the highest electron density (2×10^{10} cm^{-3}) and the lowest electron temperature (~ 0.9 eV).

Decay of OSD is a separate subject that has been extensively studied experimentally and theoretically in the context of radiative transfer in the terrestrial atmosphere [1,26] and later in the context of the models for efficient OSD production [14,17]. The decay results from a superposition of many collisional processes, besides the magnetic dipole interaction that lead to spontaneous transition with very low probability. The quenching effect on OSD of major component in the processed gas is given in Table 2. Most important processes ordered by significance in the post-discharge regime are:

(a) quenching by atomic oxygen $O_2\left(^1\Delta\right)+O\rightarrow O_2+O$

(b) quenching by ozone $O+O_2+M\rightarrow O_3+M$

$O_2(^1\Delta)+O_3\rightarrow 2O_2+O$

(c) energy pooling involving two OSD molecules $O_2\left(^1\Delta\right)+O_2\left(^1\Delta\right)\rightarrow 2\,O_2$

(d) quenching by oxygen $O_2\left(^1\Delta\right)+O_2\rightarrow 2\,O_2$ or

$O_2\left(^1\Delta\right)+O+O_2\rightarrow\ O_2+O_3$

Table 2. Quenching Effect on OSD at room temperature

Gas	Quenching rate k_q [cm^{-3}molec^{-1}s^{-1}]	Ref.
He	8.00×10^{-21}	[27]
O_2	1.54×10^{-18}	[27]
O_3	4.40×10^{-15}	[27]
OSD	1.40×10^{-17}	[27]
O	2×10^{-16}	[28]
$O + O_2$	1-2.5 $\times10^{-32}$cm^{6}s^{-1}	[26]

Weak spontaneous decay of OSD to ground state leads to very large variations in the estimated Einstein coefficients [26]. Reported values for OSD are (1.1-3.7) $\times10^{-4}$ s^{-1}, corresponding to lifetimes from 2700 s to 9000 s [20, 26]. This large uncertainty results from difficulties in calculation of magnetic dipole interaction of electrons in molecular oxygen, as well as from difficulties for isolating the radiative decay process from collisional processes that are present even at moderate pressures. For instance, for atmospheric gases Badger *et al.* [29] give the expression for the "effective" Einstein coefficient, which we modified to include small contribution of diluents gases (helium or argon),

$$A_{eff}=\left(2.6\times10^{-4}\ s^{-1}\right)\left(1+3.8P_{O_2}+3.0P_{CO_2}+0.7P_{N_2}+0.02P_{He,Ar}\right)$$

where partial pressures of individual species are given in atmospheres.

3. Detection of Molecular Metastable Oxygen

Spectroscopic techniques for OSD detection can be classified as: (a) threshold ionization mass spectroscopy (TIMS), (b) near-infrared emission spectroscopy, and (c) absorption spectroscopy.

TIMS is the oldest technique applied in the detection of OSD [4]. In a refined form it was used recently by Pulpytel *et al.* [20] to resolve and measure excited molecular oxygen states OSD and OSS during plasma-assisted chemical vapor deposition of tin oxide (SnO_2) thin films. They were able to measure accurately the appearance potentials of $O_2^+(X^2\Pi_g)$ ions from ground state (11.8±0.2 eV), OSD (11.0±0.2 eV) and OSS (10.0±0.2 eV). Threshold of their mass spectroscopy signal was below 7 eV, suggesting the presence of other metastable states ($c^1\Sigma_u^-$) and possibly of higher electronically excited states.

Transition from OSD to ground state is followed by the emission of a band system with the (0-0) transition at about 1.27 and (0-1) at 1.07 μm [30]. (0-0) vibrational band has the strongest branch, Q, centered at 1.27 μm while the ^OP branch is red-shifted and ^SR branch is blue-shifted. Absolute emission spectroscopy of the (0-0) band has been used as one of the techniques to derive the quantitative estimate of OSD number density [19]. This is a very weak band and its measurement is confronted with uncertainties in the values of Einstein coefficients [26], small signal-to noise ratio [19] and strong collisional continuum of multiple origins in the background [29]. It results in large uncertainty in estimation of OSD population in the plasma.

Spectroscopic systems involving OSD and OSS have been used to detect these species in most of the listed applications. Absorption spectroscopy in the near-infrared provides an appealing method and a variety of sensitive absorption-based laser techniques are available, including the direct-absorption spectroscopy using the long-path multipass cells [31], wavelength modulation spectroscopy [32], cavity-ringdown spectroscopy [33], cavity-enhanced absorption spectroscopy [34], ICOS [35] and the off-axis ICOS [36].

Off-axis ICOS has been used to quantitatively detect OSD generated in a variety of intra- and extra-cavity discharges. This was accomplished by recording the recently observed (0,1) band of the $b^1\Sigma_g^+$- $a^1\Delta_g$ Noxon system [37,38] suitably located in the available wavelength domain of the ICOS system. A single-mode, fiber-pigtailed DFB diode laser (1505 nm, 0.0001cm^{-1} bandwidth) is coupled into the optical cavity in an off-axis alignment that is optimized to maximize the light reentrant condition and minimize coherent interferences. The laser is temperature–controlled to set its central wavelength and then current-tuned over the singlet oxygen absorption line, ~ 0.02 cm^{-1} at 60 Hz. Light exiting the cavity is focused onto a custom, amplified InGaAs detector, and the cavity transmission is recorded as function of laser frequency. Laser wavelength calibration and the tuning domain were determined by using known water absorption lines and a calibrated SiO_2 etalon [37]. The tuning domain is sufficiently wide to scan a single, pressure broadened rotational transition in the (0,1) Noxon system. It has been demonstrated that several lines belonging to the Q and P branch of the band could be detected and scanned, which enabled accurate evaluation of the rotational temperature. Combining the measured line profiles, the rotational temperature and the transition probabilities and line strength factors from ab-initio calculations it is possible to determine the concentration of OSD in the cavity.

We used off-axis ICOS to quantitatively detect the $a^1\Delta_g$ state of O_2 via the hitherto unobserved (1,0) band of the $b^1\Sigma_g^+$-$a^1\Delta_g$ Noxon system. This approach allows for the quantitative detection of singlet O_2 with a minimum detectable density of $4x10^{13}$ molecule cm^{-3} at 298 K corresponding to $3x10^{12}$ molecule cm^{-3} per quantum state. Off-axis ICOS is convenient because it allows narrowband, continuous-wave lasers to be used in conjunction with optical cavities in a simple and effective manner [36,39]. The absorption signal is obtained through the temporal integration of the laser intensity transmitted through the cavity in the same fashion as in conventional absorption measurements. The absorption due to the medium inside the cavity is determined from the cavity output, i.e. laser transmission, which is a function of the mirror reflectivity as well as scattering and absorption losses between the mirrors [39]. The afterglow from the OSD-generating plasma (microwave discharge in Evenson cavity) passed through a coupling and through the off-axis ICOS

measurement system at about 3000 sccm and a variable total pressure. Coupling device is either a quartz tube with or without a frit, or a 5 cm Teflon® tube. Frit was used to filter out water molecules and OH radicals. The off-axis ICOS system consisted of an 82-cm long high-finesse optical cavity bounded by two highly reflective mirrors (R=99.9986%). The mirror reflectivity is determined by performing a cavity-ring down measurement [40]. Ringdown time constant is up to 250 μs (see Fig. 2a). The exact laser frequency and tuning rate are determined by using known water absorption features and a calibrated SiO_2 etalon. The ambient water spectrum is taken after the off-axis ICOS cell is filled with about 5 Torr of ambient laboratory air. The lines appearing in the spectrum are easily assigned to known water transitions using the HITRAN96 database [41]. Diode laser output is tuned by changing the temperature of the case to the wavelength range of a particular transition between the rotational levels of the Q branch of the Noxon $a^1\Delta_g \rightarrow b^1\Sigma_g^+$ (1,0) band. In addition, the laser output is fine-tuned over 2 GHz frequency range in order to scan the Doppler and pressure-broadened rotational lines. This iss accomplished by supplying a saw-tooth current ramp to the laser current source, while holding the laser case temperature constant. For calibration purpose, beam is directed prior and after the set of spectral measurements through a fused-silica etalon. Repetition rate of the saw-tooth pulse (laser wavelength tuning rate) is always kept at least an order of magnitude smaller than the characteristic cavity frequency. However, too low repetition rate distorts the symmetry of the line profile. This effect is observed in most recorded line profiles, but the error due to line profile distortion could be reduced to less than 2% by choosing carefully the sweep parameters.

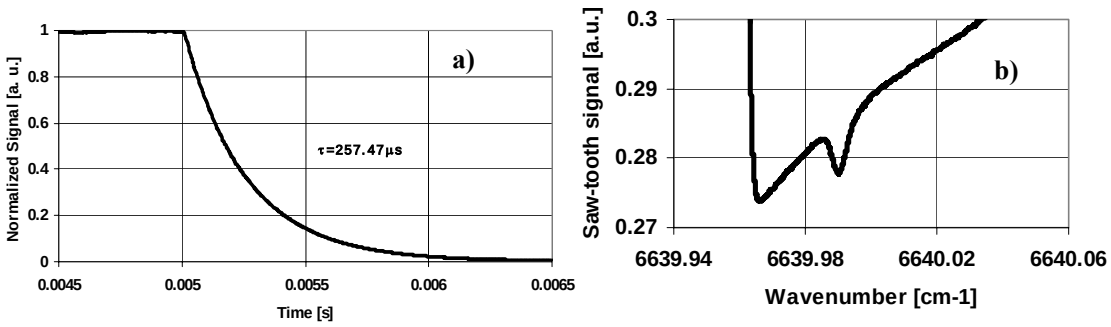

Figure 2. a) Measured ringdown decay signal. The ringdown time τ = 257.47 μs is obtained using the exponential fit of the decay signal between 0.1 and 0.9 with an error less than 0.1%;
b) Spectral signature of the Q(8) line in the Noxon band after the frequency and amplitude recalibration.

Typical line spectrum at this stage of analysis is given in Fig. 2b.

Absorption lines shown in Fig. 2c were fitted with Voigt profiles using the approximate procedure derived by Whiting [42]. First approximation is the linear combination of Gaussian and Lorentz profiles. Correcting for most of the error for the case when Gaussian and Lorentz profile have equal width and applying the quadratic variation of this correction between the end cases (no Gaussian or no Lorentz component obtains second approximation).

Voigt profile fitting techniques have been improved since the Whiting approximation was derived [43-46]. We adopted here this approach because it is relatively simple and produces less error in approximating the actual line profile than we already have due to the line scanning technique. Using the exact procedure would complicate evaluation of the yield and would not improve the overall experimental accuracy.

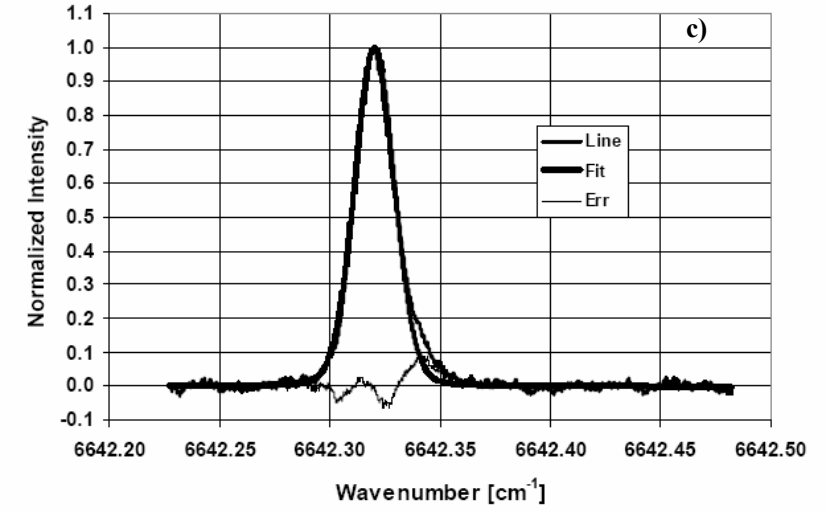

Figure 2. c) Absorption line profile of Q(4) at 300 sccm flow of oxygen and 3000 sccm flow of helium. Discharge parameters: E/N = 20.76 Td, p = 16.1 Torr, T =550 K. Ratio of Lorentz to Voigt profile $\Delta\omega_L/\Delta\omega_V$ =0.11 indicates dominant temperature (Doppler) broadening mechanism. Central wavenumber ω_0=6642.3202 cm^{-1}. Fitting error ~2%.

The fitting procedure not only gives an accurate analytical approximation, but also gives the information on the contribution of the two dominant broadening mechanisms: Doppler broadening due thermal motion of molecules (Gaussian profile) and pressure broadening (Lorentz profile). In present fitting procedure we have taken the actual FWHM as $\Delta\omega_V$ and used $\Delta\omega_L/\Delta\omega_V$ as a free parameter to fit to the recorded absorption profile. Typical result is given in Fig. 2c. In most cases Doppler broadening is dominant, and the Gaussian FWHM is much larger than Lorentzian. In this particular case, Lorentz component can be accounted for not more than 11% of the Voigt profile. Integral residual is about 2%, completely due the error in sweeping procedure.

Experimental apparatus used for production and measurement of absolute concentrations and yields of OSD at variable discharge and flow conditions is given in Fig. 3. Our estimate of active discharge region in the Evenson cavity reactor is based on the observation of oxygen triplet [4S*3p→4S*3s] at 777.19 nm. We observed that this excited state was very rapidly quenched downstream and could serve as a relatively good indicator for discharge size. Based on this observation, overall discharge length was about 1 cm. In the pressure range 10 to 60 Torr at flow rate of 3000 sccm the linear velocity in the discharge reactor was in the range of 900 to 4000 cm/s, which gave the residence time between 0.25 and 1.1 ms. We note here that Davis *et al.* [47] estimated residence time of 0.2 ms in an oxygen-argon mixture at 1 to 5 Torr, with linear flow velocity of 1100 cm/s.

4. Results and Discussion

Specific energy deposition into the discharge and the reduced electric field are the main quantitative parameters describing the processes leading to production of OSD. We will present our result by

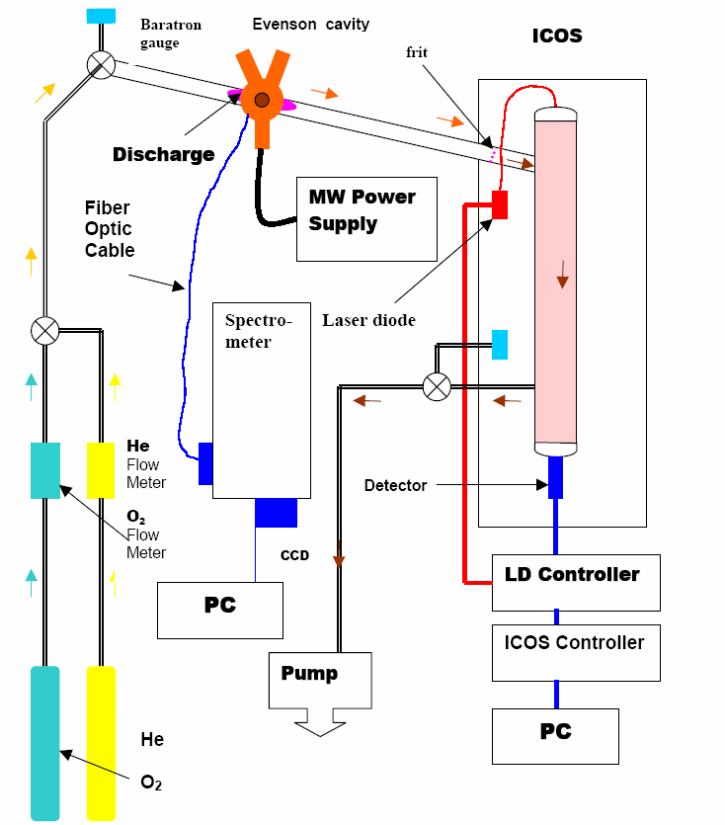

Figure 3. Schematic diagram of OSD production and detection apparatus.

plotting the specific yield of OSD versus these two parameters. We evaluated the energy per oxygen molecule and the reduced electric field from measured parameters, such as flow of Oxygen and Helium fractions, forward and reflected power, and gas-kinetic temperature and electron temperature in the discharge and in the cell. It was assumed that the electric field was constant over the discharge-cross section.

Intensity of the rotational lines measured using off-axis ICOS can be used to evaluate total population of a gas species in a particular electronic state (in present case the OSD) is given by

$$N_T = \frac{-\ln\left(1-\dfrac{\Delta I/I}{G(1-\Delta I/I)}\right)}{f\sigma L}$$

where $\Delta I/I$ is the normalized line intensity, G is the cavity enhancement factor, $\sigma(\nu)$ is the photo-absorption cross-section at given frequency, f is the oscillator strength for the particular transition, and L is the length of the cavity.

Based on the measurement of the Q(4) line shown in Fig. 3c, we obtained total number density of OSD. Yield is then calculated from

$$Y = \frac{N_T}{N} = N_T \frac{kT}{p}\frac{f_{O_2}+f_{He}}{f_{O_2}} = 1.036\times10^{19} N_T \frac{T}{p}\frac{f_{O_2}+f_{He}}{f_{O_2}}$$

where the pressure p is given in Torr, temperature T in K, and flow rates f_{O_2}, f_{He} in sccm. In this case, T = 299±6 K, measured in the cell using Boltzmann plot of absorption line intensities from Q(2) through Q(16).

Specific energy deposition is given by

$$E_0 = \frac{P}{NvA} \cong 3.49 \frac{P_F - P_R}{f_{O_2}}$$

where P is the power absorbed by the discharge, N is the number density of oxygen molecules, v is the flow speed, A is the cross-section area, and P_F, P_R are the forward and reflected power, respectively.

Figure 4 shows the OSD yield as a function of specific energy deposition. By comparison, the same plot obtained by Stafford and Kushner [14] has a maximum slightly shifted toward lower energy. They have performed a computational experiment where a set of 256 most probable discharge conditions were factorized and specific deposited energy and OSD yield was computed. Both parameters have universal meaning and value, independent from discharge type. In Fig. 4 only the upper and lower values of data were compared with present experiment. The maximum of experimental data is not so well pronounced, probably due to the fact that the experimental energy range was limited, and did not exceed 12 eV. The trend seems to be shifted by 1-2 eV, which is probably due to inaccurate value of the relative probability of oxygen inelastic collisions incorporated in the experimental evaluation of the specific energy. However, we found that the results of Ref. [14] is reproduced qualitatively, and both oxygen-"rich" and oxygen-"lean" mixtures show the yield that follows the same trend. The diagram shows that the low yield in the oxygen-"rich" mixtures is due to a low level of the specific energy deposition, and that density-induced yield reduction is probably an effect of secondary importance. More data are needed in order to justify this conclusion and to fill the gap between the oxygen-"rich" and oxygen-"lean" data. OSD yield data obtained in present experiment are substantially lower than the upper limit in the computational experiment data. The discrepancy is larger than the experimental error. We found no systematic error in our measurement techniques that would compensate for this disagreement. Rather, our experiment seems to reconfirm the tendency of current models to overestimate the OSD yield [33].

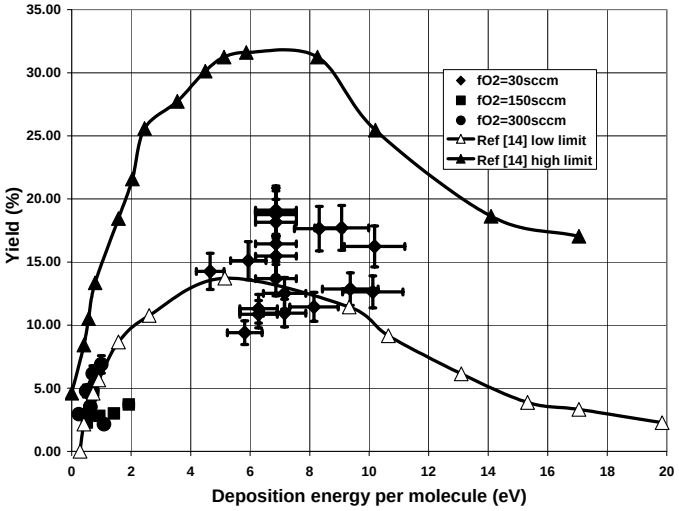

Figure 4. OSD yield as a function of specific energy deposition in Oxygen molecules. Solid lines: envelopes of the factorial computational experiment data of Ref. [14]. Error in present experimental data is due to uncertainties in electron and gas-kinetic temperature, and estimated uncertainty of constant field approximation.

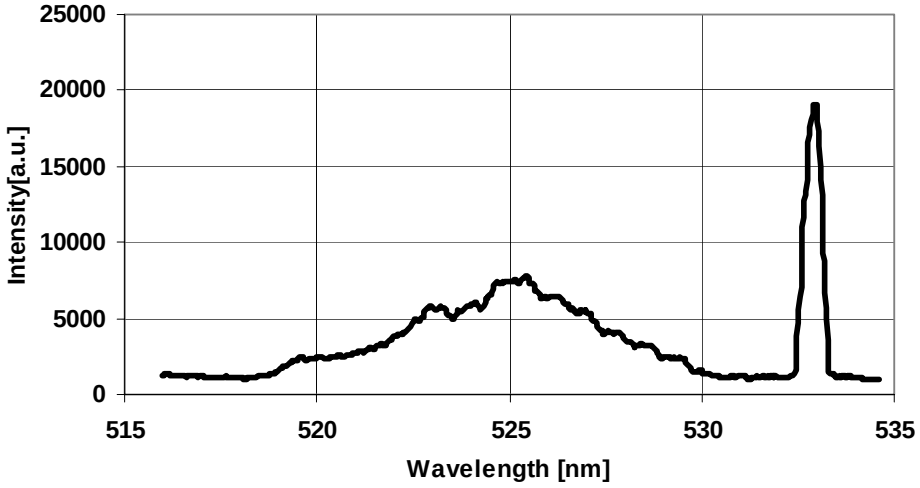

Figure 5. Spectrum of the He/O_2 discharge showing simultaneous emission of a system of molecular oxygen ion bands from the $^4\Sigma_g^- \rightarrow {}^4\Pi_u$ system around 520 nm, and the $^5P\text{-}^5D^o$ atomic oxygen emission at 533.07 nm.

Models of oxygen-noble-gas plasmas usually take into account a limited number of oxygen specii (ground states and some metastables). Analysis of the effect of other excited specii is necessary. For example, we observed strong emission bands of molecular oxygen ions together with strong spectral lines of atomic oxygen as shown in Fig. 5. It seems to be a vigorous dynamics of these states that depends strongly on the oxygen content in the discharge as shown in Fig. 6.

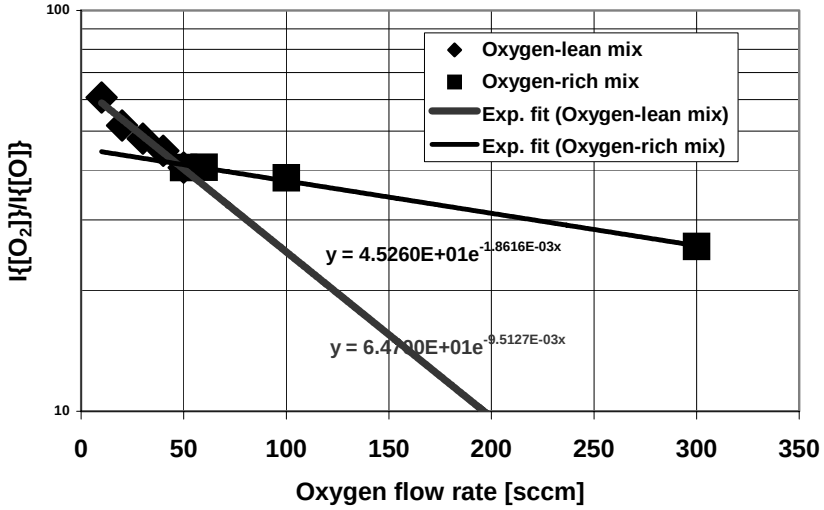

Figure 6. Ratio of molecular ion band integral intensity ($^4\Sigma_g^- \rightarrow {}^4\Pi_u$ system) to the atomic line ($^5P\text{-}^5D^o$) intensity at Helium flow rate of 3000 sccm.

Additional source of discrepancy could be a possible thermal dissociation through the vibrationally excited metastable $c^1\Sigma_u^-$ state. The lowest vibrational level of this state has dissociation

energy of about 0.8 eV. Thermal dissociation mechanism is responsible for elimination of OSD from thermal plasmas, such as MW torches [48].

5. Production of Metastable Atomic Oxygen from Arc-seeded MW Plasma Torch

Recently, considerable attention was given to the development of plasma sources that produce atmospheric pressure plasma in air, since such plasmas can be used in open space for various applications. A portable arc-seeded microwave plasma torch running stably with airflow is an excellent source of reactive oxygen species that can be used as an ignition aide for hydrocarbon fuel super-sonic combustor or as a device that can effectively oxidize biological agents [48-51]. Later application is especially important for objects that could not be treated thermally or with wet chemistry treatment. The reactive oxygen species are produced and carried in the air plasma effluents to the exposed object. Relative concentration of reactive oxygen species can be determined by the emission spectroscopy. A spatial distribution of atomic oxygen was determined under the different flow conditions and presented in this paper.

Our plasma source combines an arc torch module with a rectangular microwave cavity in the form of a microwave adaptor. The torch module is used not only to generate the arc plasma but also to couple the microwave power from the cavity to the arc plasma for microwave enhancement. Detailed description of the apparatus, electrical characteristics, and plasma diagnostic can be found in [48-51].

The dynamics and distribution of atomic oxygen in the discharge was monitored by observing the atomic oxygen (OI) lines in the spectral region between 777.1 and 777.6 nm, namely $^5P(J=3)$ - $^5S^o(J=2)$ transition at ~777.19 nm, $^5P(J=2)$ - $^5S^o(J=2)$ transition at ~777.42 nm, and $^5P(J=1)$-$^5S^o(J=2)$ transition at ~777.54 nm, as shown in Fig. 8. Molecular emission spectrum of nitrogen was practically nonexistent, compared with the spectral intensity of the OI lines. Strong emission from molecular oxygen was observed in remote, cooler regions of the torch.

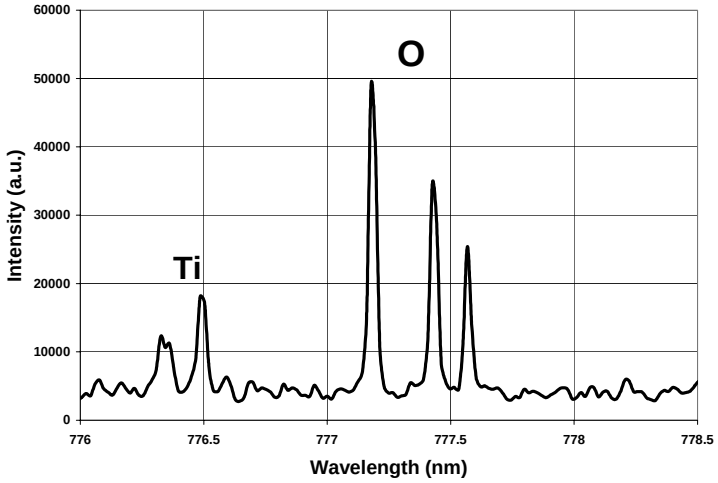

Figure 7. Emission spectrum in the region from 776 – 778.5 nm emitted from the torch at 2 cm above the surface of the waveguide.

The dependence of atomic oxygen content in the torch on the air supply pressure (i.e., flow rate) is illustrated in Fig. 8a. It is shown that oxygen content (i.e intensity of OI emission) increases as the flow rate increases. The required breakdown field for the discharge increases with the flow rate, thus more energetic electrons is produced as the flow rate increases. These energetic electrons dissociate oxygen molecule more efficiently.

Lateral distribution of OI emission for different vertical positions is shown on the Fig. 8b. It can be observed that the shape of lateral distribution depends on the vertical position of observational point. With increase of the vertical distance from the surface of waveguide minimum of the irradiance around center of discharge becomes deeper. That can be explained by "loop" like shape of plasma presented on the images in Ref.52. Same explanation can be given for shifting the maximum of irradiance that can be observed with the change of the vertical observational position.

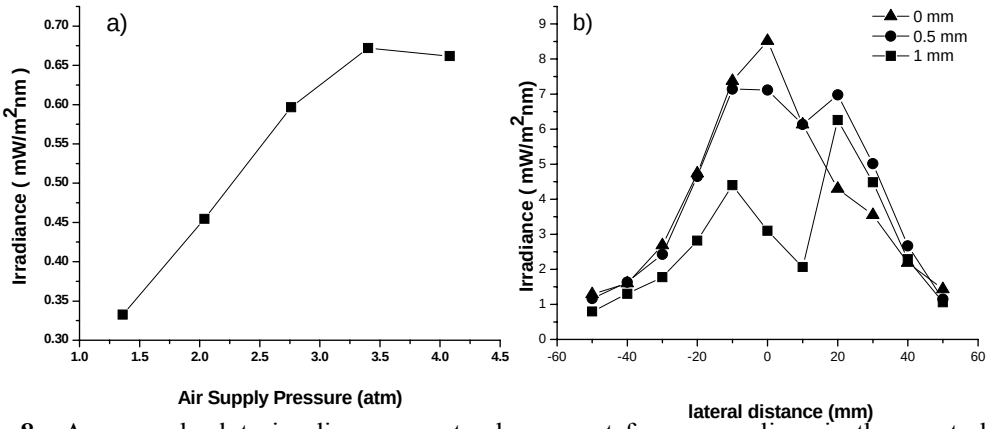

Figure 8. Average absolute irradiance over torch segment for oxygen lines in the spectral region between 777.1 and 777.6 nm dependence on: a) air supply pressure for 2 mm above the surface of waveguide, b) spatial position.

6. Conclusion

While reviewing previous modeling and experimental work on the production of metastable oxygen molecules and atoms we observed that the competitive molecular and atomic oxygen kinetics in electric discharges can give quite different results, depending on the gas temperature in the discharge. In order to further elucidate this observation we compiled our results from two different discharges, the MW cavity discharge, and the arc-seeded microwave torch. In the microwave cavity discharge, the rotational temperature was rather low, between 300 and 600 K. Singlet $O_2(^1\Delta)$ was produced by microwave cavity discharge of He/O_2 mixture in a wide range of gas and plasma parameters. In the arc-seeded microwave torch heavy particle temperature exceeded 2000 K. The kinetics in two discharges is completely different, one leading to high yield, and the other to low yield of OSD.

In the MW cavity experiment special attention was given to the measurement of OSD concentration. Integrated – cavity off-axis ring down spectroscopy (ICOS) was further developed for sensitive detection of singlet $O_2(^1\Delta)$. Maximum yield of OSD obtained in the MW cavity experiment was as much as 19%, with apparent maximum in the same domain of specific energy as in the factorial computational experiments.

Emission spectroscopy is used simultaneously with the ICOS technique, in order to characterize the discharge and compare the discharge parameters with the OSD yield. Discharge dynamics are monitored by obtaining the line intensity ratio. We concluded that, in addition to the reduced electric field, major factors that affecting the kinetics were pressure and oxygen content. We make a clear distinction between the behavior of line intensities in oxygen-"lean" (low mole fraction) and oxygen-"rich" (higher mole fraction) mixtures. Another useful indicator of discharge kinetics is the relative ratio of the molecular ion band intensity to the atomic oxygen line intensity. Oxygen ion band emission is enhanced by helium. Some bands of the First Negative system are especially intensive. They are observed simultaneously with the atomic oxygen lines in the common spectral

frame. We found that the ratio of integral band to the integral line intensity drops with the absorbed power.

Emission spectra from the arc seeded microwave torch in air show that the dominant radiation was from the atomic oxygen lines, and that nitrogen and oxygen molecular bands are virtually nonexistent.

References

[1] Mlynczak M G and Marshall B T 1996 *Geophys. Res. Lett.* **23** 657-660
[2] Harney M A, Hess D W and Soane D S 1989 *J. Vac. Sci. Technol.* **B7** 1-13
[3] Hermann H W, Henins I, Park J and Selwyn G S 1999 *Phys. of Plasmas* **6** 2284-2289
[4] Foner S N and Hudson R L 1956 *J. Chem. Phys.* **25** 601-602
[5] Wood R W 1920 *Proceedings of the Royal Society of London, Ser. A* **97** 455-470
[6] Pearce R W B and Gaydon A G 1950 *The Identification of Molecular Spectra* (London: Willey)
[7] Benard D J and Pchelkin N R 1978 *Rev. Sci. Instrum.* **49** 794-796
[8] Napartovich A P, Deryugin A and Korchetov I 2001 *J. Phys. D* **34** 1827-1833
[9] Schmiedberger J and Fujii H 2001 *Appl. Phys. Lett.* **78** 2649-2651
[10] Carroll D L, Verdeyen J T and Solomon W C 2002 *US Patent No.* 6501780
[11] Rakhimova T V, Kovalev A S, Rakhimov A T, Klopovsky K S, Lopaev D V, Mankelevich Yu A,
Proshina O V, Braginsky O V and Vasilieva A N 2003 *AIAA Paper* 2003-4306
[12] Savin Y V, Goryachev L V, Adamenkov Yu A, Rakhimova T V, Mankelovich Yu A, Popov N A, Adamenkov A A, Egorov V V, Ilyin S P, Kolobyanin Yu V, Kudryazhov E A, Rogozhnikov G S and B A Vyskubenko 2004 *J. Phys. D* **37** 3121-3128
[13] Ionin A A, Klimachev Y M, Kotkov A A, Kochetov I V, Napartovich A P, Seleznev L V, Sinitsyn D V and Hager G D 2003 *J. Phys. D* **36** 982-989
[14] Stafford D S and Kushner M J 2004 *J. Appl. Phys.* **96** 2451-2465
[15] Carroll D L, Verdeyen J T, King D M, Zimmerman J W, Laystrom J K, Woodard B S, Benavides G F, Kittel K, Stafford D S, Kushner M J and Solomon W C 2005 *Appl. Phys. Lett.* **86** 111104(3 pages)
[16] Carroll D L, Verdeyen J T, King D M, Zimmerman J W, Laystrom J K, Woodard B S, Richardson N, Kittel K, Kushner M J and Solomon W C 2004 *Appl. Phys. Lett.* **85** 1320-1322
[17] Stafford D S and Kushner M J 2005 *J. Appl. Phys.* **98** 073303(12 pages)
[18] Arakoni R, Stafford D S, Babaeva N Y and Kushner M J 2005 *J. Appl. Phys.* **98** 073304(7 pages)
[19] Rawlins W T, Lee S, Kessler W J and Davis S J 2005 *Appl. Phys. Lett.* **86** 051105(3 pages)
[20] Pulpytel J, Arefi-Khonsari F and Morscheidt W 2005 *J. Phys. D* **38** 1390-1395
[21] Carroll D L, Verdeyen L T, King D M, Zimmerman J W, Laystrom J K, Woodard B S, Benavides G F and Kittel K 2005 *IEEE J. Quant. Electronics* **41** 213-223
[22] Babaeva N Y, Akaroni R A and Kushner M J 2006 *J. Appl. Phys.* **99** 113306(11 pages)
[23] Verdeyen J T, Carroll D L, King D M, Zimmerman J W, Laystrom J K, Woodard B S, Benavides J F, Kittel K, Stafford D S, Kushner M J and Solomon W C 2006 *Appl. Phys. Lett.* **89** 101115(3 pages)
[24] Ionin A A, Napartovich A P and Yurichev N N 2006 *Laser Phys.* **16** 155-172
[25] Proshina O V, Rakhimova T V, Braginsky O V, Kovalev A S, Lopaev D V, Mankelevich Yu A, Rakhimov A T and Vasilieva A N 2006 *J. Phys. D* **39** 5191-

5200
[26] Ionin A A, Kochetov I V, Napartovich A P and Yurichev N N 2007 *J. Phys. D* **40** R25-R61
[27] Okabe H 1978 *Photochemistry of Small Molecules* (New York: Willey-Interscience)
[28] Herron J T and Green D S 2001 *Plasma Chem. Plasma Process.* **21** 459-481
[29] Badger R M, Wright A C and Whitlock R F 1965 *J. Chem. Phys*. **43** 4345-4351
[30] Herzberg G 1950 *Molecular Spectra and Molecular Structure, I: Spectra of Diatomic Molecules*, p. 233-235 (New York: Van Nostrand)
[31] McManus J B, Kebabian P I and Zahniser M S 1995 *Appl. Opt.* **34** 3336-3348
[32] Silver J A 1992 *Appl. Opt.* **31** 707-717
[33] O'Keefe A and Deacon D A G 1988 *Rev. Sci. Instrum.* **59** 2544-2551
[34] Engeln R, Berden G, Peeters R and Meijer G 1998 *Rev. Sci. Instrum.* **69** 3763-3769
[35] O'Keefe A 1998 *Chem. Phys. Lett.* **293** 331-336
[36] Paul J B, Lapson L and Anderson J G 2001 *Appl.Opt.* **40** 4904-4910
[37] Williams S, Gupta M, Owano T, Baer D S, O'Keefe A, Yarkony D R and Matsika S 2003 *Bull. Am. Phys. Soc.* (56th GEC) **48** WF1 4
[38] Noxon J F 1961 *Can. J. Phys.* **39** 1110-1119
[39] O'Keefe A, Scherer J J and Paul J B 1999 *Chem. Phys. Lett.* **307** 343-349
[40] Baer D S, Paul J B, Gupta M and O'Keefe A 2002 *App. Phys. B* **75** 261-265
[41] Rothman L S, Rinsland C P, Goldman A, Massie S T, Edwards D P, Mandin J -Y, Schroeder J, Mc-Cann A, Gamache R R, Wattsin R B, Yoshino K, Chance K V, Juck K W, Brown L R, Nemtchechin V and Varanasi P 1998 *J. Quant. Spec. Radiat. Transf.* **60** 665-710
[42] Whiting E E 1968 *J. Quant. Spec. Radiat. Transf.* **8** 1379-1384
[43] Hui A K, Armstrong B H and Wray A A 1978 J. *Quant. Spec. Radiat. Transf.* **19** 509-516
[44] Humlicek J 1979 *J. Quant. Spec. Radiat. Transf.* **21** 309-313
[45] Humlicek J 1982 *J.Quant. Spec. Radiat. Transf.* **27** 437-444
[46] Zhu X 1988 *J. Quant. Spec. Radiat. Transf.* **39** 421-427
[47] Davis S J, Rawlins W T, Seonkyung L, Silva M L, Kessler W J and Mulhall P A 2004 *Proceedings of SPIE* 5448-865
[48] KuoS P, Bivolaru D, Lai H, Lai W, Popović S and Kessaratikoon P 2004 *IEEE Trans. Plasma Sci.* **32** 1734-1741
[49] Rašković M, Popović S, Kuo S P and Vušković L 2006 *23rd Summer School and International Symposium on the Physics of Ionized Gases, Book of Contributed Papers,* p. 487 (Belgrade: Institute of Physics)
[50] Kuo S P, Rubinart M, Popović S and Bivolaru D 2006 *IEEE Trans. Plasma Sci.* **34** 2537-2544
[51] Kuo S P, Tarasenko), Popović S and Levon K 2006 *IEEE Trans. Plasma Sci.* **34** 1-8
[52] Kuo S P, Rubinart M, Popović S and Bivolaru D 2006 *AIAA* Paper 2006-1446